

1237 **Chapter 3**
1238 **Classical Cyclotron**

1239 **Abstract** This chapter introduces the classical cyclotron, and the theoretical material
1240 needed for the simulation exercises. It begins with a brief reminder of the historical
1241 context, and continues with beam optics and with the principles and methods which
1242 the classical cyclotron leans on, including
1243 - ion orbit in a cyclic accelerator,
1244 - weak focusing and periodic transverse motion,
1245 - revolution period and isochronism,
1246 - voltage gap and resonant acceleration,
1247 - the cyclotron equation.

1248 The simulation of a cyclotron dipole will either resort to an analytical model of the
1249 field: the optical element DIPOLE, or will resort to using a field map together with
1250 the keyword TOSCA to handle it and raytrace through. An additional accelerator
1251 device needed in the exercises, CAVITE, simulates a local oscillating voltage. Run-
1252 ning a simulation generates a variety of output files, including the execution listing
1253 zgoubi.res, always, and other zgoubi.plt, zgoubi.CAVITE.out, zgoubi.MATRIX.out,
1254 etc., aimed at looking up program execution, storing data for post-treatment, produc-
1255 ing graphs, etc. Additional keywords are introduced as needed, such as the matching
1256 procedure FIT[2]; FAISCEAU and FAISTORE which log local particle data in
1257 zgoubi.res or in a user defined ancillary file; MARKER; the 'system call' command
1258 SYSTEM; REBELOTE, a 'do loop'; and some more. This chapter introduces in addi-
1259 tion to spin motion in accelerator magnets; dedicated simulation exercises include a
1260 variety of keywords: SPNTRK, a request for spin tracking, SPNPRT or FAISTORE,
1261 to log spin vector components in respectively zgoubi.res or some ancillary file, and
1262 the "IL=2" flag to log stepwise particle data, including spin vector, in zgoubi.plt file.
1263 Simulations include deriving transport matrices, beam matrix, optical functions and
1264 their transport, from rays, using MATRIX and TWISS keywords.

1265 **Notations used in the Text**

$B; B_0$	magnetic field; at a reference radius R_0
$\mathbf{B}; B_R; B_y$	field vector; radial component; axial component
$BR = p/q$	magnetic rigidity
$C; C_0$	orbit length, $C = 2\pi R$; reference, $C_0 = 2\pi R_0$
E	ion energy, $E = \gamma m_0 c^2$
$f_{\text{rev}}, f_{\text{rf}}$	revolution and RF voltage frequencies
G	gyromagnetic anomaly, $G = 1.7928$ for proton, -4.184 for helium
h	harmonic number, an integer, $h = f_{\text{rf}}/f_{\text{rev}}$
$k = \frac{R}{B} \frac{dB}{dR}$	radial field index
$m; m_0; M$	ion mass; rest mass; in units of MeV/c^2
$\mathbf{p}; p; p_0$	ion momentum vector; its modulus; reference
q	ion charge
$R; R_0; R_E$	equilibrium orbit radius; reference, $R(p_0)$; at energy E
RF	Radio-Frequency
1266 s	path variable
$T_{\text{rev}}, T_{\text{rf}}$	revolution and accelerating voltage periods
$\mathbf{v}; v$	ion velocity vector; its modulus
$V(t); \hat{V}$	oscillating voltage; its peak value
W	kinetic energy, $W = \frac{1}{2}mv^2$
x, x', y, y'	radial and axial coordinates $\left[(*)' = \frac{d(*)}{ds} \right]$
α	trajectory deviation, or momentum compaction
$\beta = \frac{v}{c}; \beta_0; \beta_s$	normalized ion velocity; reference; synchronous
$\gamma = E/m_0c^2$	Lorentz relativistic factor
$\Delta p, \delta p$	momentum offset
ε_u	Courant-Snyder invariant ($u : x, r, y, l, Y, Z, s, \text{etc.}$)
θ	azimuthal angle
ϕ	RF phase at ion arrival at the voltage gap

1267 **3.1 Introduction**

1268 Cyclotrons are the most widespread type of accelerator, today, used by thousands,
 1269 with the production of isotopes as the dominant application. This chapter is devoted
 1270 to the first cyclic accelerator: the early 1930s *classical* cyclotron which its concept
 1271 limited to low energy, a few 10s of $\text{MeV}/\text{nucleon}$. This limitation overcome a decade
 1272 later by the azimuthally varying field (AVF) technique, this is the subject of the next
 1273 chapter.

1274 The classical cyclotron is based on four main principles:

1275 (i) the use of a cylindrical-symmetry magnetic field in the gap of an electromagnet
 1276 (Fig. 3.1) to maintain ions on a circular trajectory

- 1277 (ii) transverse vertical confinement of the beam obtained by a slow radial decrease
 1278 of the magnetic field. A technique known as weak focusing, applied over the years
 1279 in all cyclic accelerators: microtron, betatron, synchrocyclotron, synchrotron. These
 1280 weak focusing accelerator species all are still part of the landscape today
 1281 (iii) resonant acceleration by synchronization of a fixed-frequency accelerating volt-
 1282 age on the quasi-constant revolution time (Fig. 3.1). and
 1283 (iv) use of high voltage, to mitigate the effect of the turn-by-turn RF phase slip.

1284 Resonant acceleration has the advantage that a small gap voltage is enough to
 1285 accelerate with, in principle, no energy limitation, by contrast with the electrostatic
 1286 techniques developed at the time, which required the generation of the full voltage,
 1287 such as the Van de Graaf which was limited by sparking at a few tens of megavolts.

1288 The cyclotron concept goes back to the late 1920s [?], yet it was not until the early
 1289 1930s when a cyclotron was first brought to operation [?]. The principles are sum-
 1290 marized in Fig. 3.1: an oscillating voltage is applied on a pair of electrodes (“dees”)
 1291 forming an accelerating gap and placed between the two poles of an electromagnet.
 1292 Ions reaching the gap during the acceleration phase of the voltage wave experience
 1293 an energy boost; no field is experienced inside the dees. Under the effect of energy
 1294 increase at the gap every half-revolution, they spiral out in the quasi-constant field
 of the dipole.

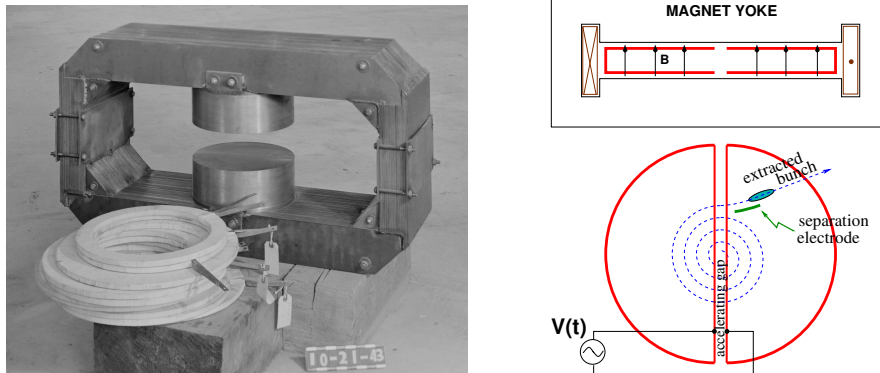


Fig. 3.1 Left: a cyclotron electromagnet, namely here that used for a model of Berkeley’s 184-inch cyclotron in the early 1940s [?]. Magnetic field in the gap decreases with radius. Right: a schematic of the resonant acceleration motion; gap after gap, accelerated ions spiral out (bottom) in the quasi-uniform field (top). A double-dee (or, a variant, a single-dee facing a slotted electrode) forms an accelerating gap. The fixed-frequency oscillating voltage $V(t)$ applied is a harmonic of the revolution frequency. Ions experiencing proper voltage phase at the gap, turn by turn, are accelerated. A septum electrode allows beam extraction

1295 The first cyclotron achieved acceleration of H_2^+ hydrogen ions to 80 keV [?], at
 1296 Berkeley in 1931. The apparatus used a dee-shaped electrode vis-à-vis a slotted
 1297 electrode forming a voltage gap, the ensemble housed in a 5 in diameter vacuum
 1298 chamber and placed in the 1.3 Tesla field of an electromagnet. A ≈ 12 MHz vacuum
 1299 tube oscillator provided 1 kVolt gap voltage.
 1300

1301 One goal foreseen in developing this technology was the acceleration of protons
 1302 to MeV energy range for the study of atom nucleus. And in background, a wealth
 1303 of potential applications. An 11 in cyclotron followed which delivered a $0.01 \mu\text{A}$
 1304 H_2^+ beam at 1.22 MeV [?], and a 27 in cyclotron later reached 6 MeV (Fig. 3.2) [?].
 1305 Targets were mounted at the periphery of the 11-inch cyclotron, disintegrations were
 1306 observed in 1932. And, in 1933: *'The neutron had been identified by Chadwick*
 1307 *in 1932. By 1933 we were producing and observing neutrons from every target*
 1308 *bombarded by deuterons.*“ [?, M.S. Livingston, p. 22].

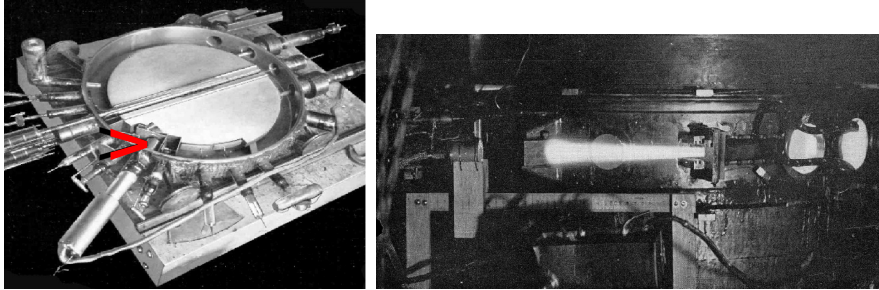
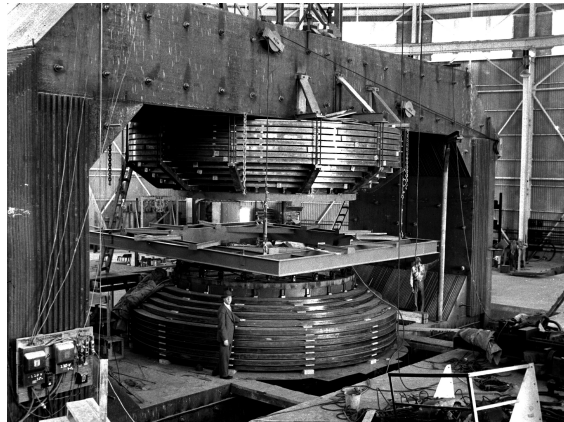


Fig. 3.2 Berkeley 27-inch cyclotron, brought to operation in 1934, accelerated deuterons up to 6 MeV. Left: a double-dee (seen in the vacuum chamber, cover off), 22 in diameter, creates an accelerating gap: 13 kV, 12 MHz radio frequency voltage is applied for deuterons for instance (through two feed lines seen at the top right corner). This apparatus was dipped in the 1.6 Tesla dipole field of a 27 in diameter, 75 ton, electromagnet. A slight decrease of the dipole field with radius, from the center of the dipole, ensures axial beam focusing. With their energy increasing, ions spiral out from the center to eventually strike a target (red arrow). Right: ionization of the air by the extracted beam (1936); the view also shows the vacuum chamber squeezed between the pole pieces of the electromagnet [?]

Fig. 3.3 Berkeley 184 in diameter, 4,000 ton cyclotron during construction [?]. The coil windings around both of the magnetic poles are clearly visible. Following the invention of longitudinal focusing it was actually operated as a synchrocyclotron, in 1946. The man on the right gives the scale



1309 A broad range of applications were foreseen: “*At this time biological experiments*
 1310 *were started. [...] Also at about this same time the first radioactive tracer experiments*
 1311 *on human beings were tried [...] simple beginnings of therapeutic use, coming a*
 1312 *little bit later, in which neutron radiation was used, for instance, in the treatment*
 1313 *of cancer. [...] Another highlight from 1936 was the first time that anyone tried*
 1314 *to make artificially a naturally occurring radio-nuclide. (a bismuth isotope) [?,*
 1315 *McMillan, p. 26].*

1316 Berkeley’s 184 in cyclotron, the largest (Fig. 3.3), commissioned in 1941, was to
 1317 accelerate Deuterons to 100 MeV for meson production. It’s magnet however was
 1318 diverted to the production of uranium for the atomic bomb during the second world
 1319 war years [?]. Re-started in 1946, as a consequence of the discovery of phase focusing
 1320 the accelerator was actually operated as a synchrocyclotron (an accelerator species
 1321 addressed in Chap. 7).

1322 *Limitation in energy*

1323 The understanding of the dynamics of ions in the classical cyclotron took some time,
 1324 and brought two news, a bad one and a good one,

1325 (i) the bad one first: the energy limitation. A consequence of the loss of isochro-
 1326 nism resulting from the relativistic increase of the ion mass so that “[...] *it seems*
 1327 *useless to build cyclotrons of larger proportions than the existing ones [...] an accel-*
 1328 *erating chamber of 37 in radius will suffice to produce deuterons of 11 MeV energy*
 1329 *which is the highest possible [...] [?], or in a different form: “If you went to graduate*
 1330 *school in the 1940s, this inequality ($-1 < k < 0$) was the end of the discussion of*
 1331 *accelerator theory” [?].*

1332 (ii) the good news now: the energy limit which results from the mass increase can
 1333 be removed by splitting the magnetic pole into valley and hill field sectors. This is
 1334 the azimuthally varying field (AVF) cyclotron technology, due to L.H. Thomas in
 1335 1938 [?]. It took some years to see effects of this breakthrough (Fig. 3.4). The AVF
 1336 is the object of Chap. 4.

1337 With the progress in magnet computation tools, in computer speed and in beam
 1338 dynamics simulations, the AVF cyclotron ends up being essentially as simple to
 1339 design and build: it has in a general manner supplanted the classical cyclotron in all
 1340 energy domains (Fig. 3.4).

1341 **3.2 Basic Concepts and Formulæ**

1342 The cyclotron was conceived as a means to overcome the technological difficulty of
 1343 a long series of high electrostatic voltage electrodes in a linear layout, by, instead,
 1344 repeated recirculation through a single accelerating gap in synchronism with an
 1345 oscillating voltage (Fig. 3.5). As the accelerated bunch spirals out in the uniform
 1346 magnetic field, the velocity increase comes with an increase in orbit length; the

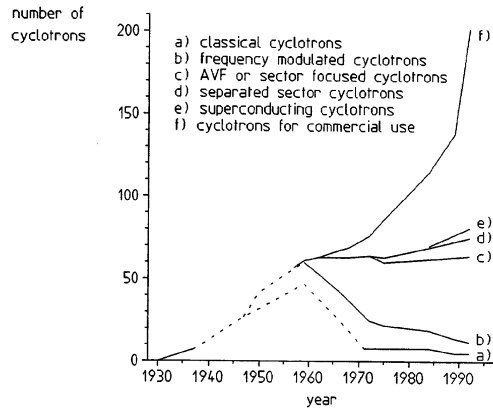


Fig. 3.4 Evolution of the number of the various cyclotron species, over the years [?]. From the 1950s on the AVF cyclotron rapidly supplanted the 1930s' classical cyclotron

Fig. 3.5 Resonant acceleration: in an $h = 1$ configuration an ion bunch meets an oscillating field \mathbf{E} across gap A, at time t , at an accelerating phase; it meets again, half a turn later, at time $t + T_{rev}/2$, the accelerating phase across gap A', and so on: the magnetic field recirculates the bunch through the gap, repeatedly. Higher harmonic allows more bunches: the next possibility in the present configuration is $h=3$, and 3 bunches, 120 degrees apart, in synchronism with \mathbf{E}

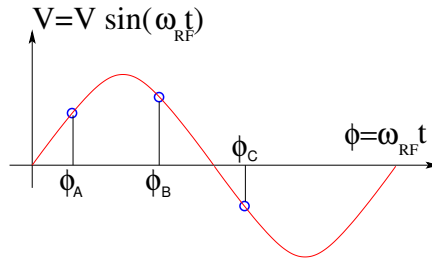
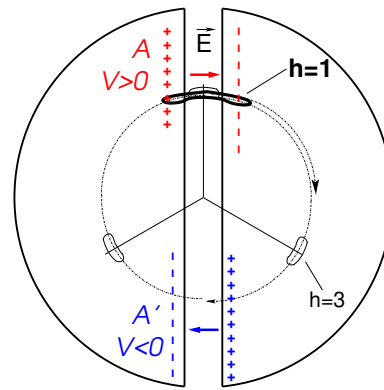


Fig. 3.6 An ion which reaches the double-dee gap at the RF phase $\omega_{rf}t = \phi_A$ or $\omega_{rf}t = \phi_B$ is accelerated. If it reaches the gap at $\omega_{rf}t = \phi_C$ it is decelerated

1347 net result is a slow increase of the revolution period T_{rev} with energy, yet, with
 1348 appropriate fixed $f_{\text{rf}} \approx h/T_{\text{rev}}$ the revolution motion and the oscillating voltage can
 1349 be maintained in sufficiently close synchronism, $T_{\text{rev}} \approx T_{\text{rf}}/h$, that the bunch will
 1350 transit the voltage gap at an accelerating phase (Fig. 3.6) over a large enough number
 1351 of turns that it acquires a significant energy boost.

1352 The orbital motion quantities: radius R , ion rigidity BR , revolution frequency
 1353 f_{rev} , satisfy

$$BR = \frac{p}{q}, \quad 2\pi f_{\text{rev}} = \omega_{\text{rev}} = \frac{v}{R} = \frac{qB}{m} = \frac{qB}{\gamma m_0} \quad (3.1)$$

1354 These relationships hold at all γ , so covering the *classical* cyclotron domain ($v \ll c$,
 1355 $\gamma \approx 1$) as well as the *isochronous* cyclotron (in which the ion energy increase is
 1356 commensurate with its mass). To give an idea of the revolution frequency, in the
 1357 limit $\gamma = 1$, for protons, one has $f_{\text{rev}}/B = q/2\pi m = 15.25 \text{ MHz/T}$.

1358 The cyclotron design sets the constant RF frequency $f_{\text{rf}} = \omega_{\text{rf}}/2\pi$ at an interme-
 1359 diate value of hf_{rev} along the acceleration cycle. The energy gain, or loss, by the ion
 1360 when transiting the gap, at time t , is

$$\Delta W(t) = q\hat{V} \sin \phi(t) \quad \text{with} \quad \phi(t) = \omega_{\text{rf}}t - \omega_{\text{rev}}t + \phi_0 \quad (3.2)$$

1361 with ϕ its phase with respect to the RF signal at the gap (Fig. 3.6), $\phi_0 = \phi(t = 0)$,
 1362 and $\omega_{\text{rev}}t$ the orbital angle. Assuming constant field B , the increase of the revolution
 1363 period with ion energy satisfies

$$\frac{\Delta T_{\text{rev}}}{T_{\text{rev}}} = \gamma - 1 \quad (3.3)$$

1364 The mis-match so induced between the RF and cyclotron frequencies is a turn-by-turn
 1365 cumulative effect and sets a limit to the tolerable isochronism defect, $\Delta T_{\text{rev}}/T_{\text{rev}} \approx$
 1366 $2 - 3\%$, or highest velocity $\beta = v/c \approx 0.22$. This results for instance in a practical
 1367 limitation to $\approx 25 \text{ MeV}$ for protons, and $\approx 50 \text{ MeV}$ for D and α particles, a limit
 1368 however dependent on energy gain per turn.

1369 Over time multiple-gap accelerating structures were developed, whereby a
 1370 “multiple- Δ ” electrode pattern substitutes to a “double-D”. An example is GANIL C0
 1371 injector with its 4 accelerating gaps and $h = 4$ and $h = 8$ RF harmonic operation [?].

1372 3.2.1 Fixed-Energy Orbits, Revolution Period

In a laboratory frame (O;x,y,z), with (O;x,z) the bend plane (Fig. 3.7), assume
 $\mathbf{B}|_{y=0} = \mathbf{B}_y$, constant. An ion is launched from the origin with a velocity

$$\mathbf{v} = \left(\frac{dx}{dt}, \frac{dy}{dt}, \frac{dz}{dt} \right) = (v \sin \alpha, 0, v \cos \alpha)$$

1373 at an angle α from the z -axis. Solving

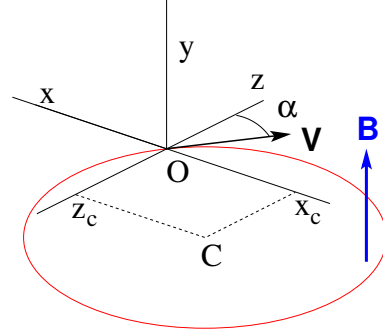


Fig. 3.7 Circular motion of an ion in the plane normal to a uniform magnetic field **B**. The orbit is centered at $x_C = -v \cos \alpha / \omega_{\text{rev}}$, $z_C = v \sin \alpha / \omega_{\text{rev}}$, its radius is v / ω_{rev}

$$m\dot{\mathbf{v}} = q\mathbf{v} \times \mathbf{B} \quad (3.4)$$

1374 with $\mathbf{B} = (0, B_y, 0)$ yields the parametric equations of motion

$$\begin{cases} x(t) = \frac{v}{\omega_{\text{rev}}} \cos(\omega_{\text{rev}}t - \alpha) - \frac{v \cos \alpha}{\omega_{\text{rev}}} \\ y(t) = \text{constant} \\ z(t) = \frac{v}{\omega_{\text{rev}}} \sin(\omega_{\text{rev}}t - \alpha) + \frac{v \sin \alpha}{\omega_{\text{rev}}} \end{cases} \quad (3.5)$$

1375 which result in

$$\left(x + \frac{v \cos \alpha}{\omega_{\text{rev}}}\right)^2 + \left(z - \frac{v \sin \alpha}{\omega_{\text{rev}}}\right)^2 = \left(\frac{v}{\omega_{\text{rev}}}\right)^2 \quad (3.6)$$

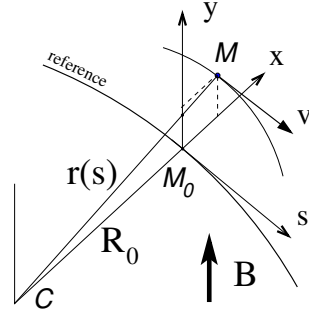
1376 a circular trajectory of radius $R = v / \omega_{\text{rev}}$ centered at $(x_C, z_C) = \left(-\frac{v \cos \alpha}{\omega_{\text{rev}}}, \frac{v \sin \alpha}{\omega_{\text{rev}}}\right)$.

1377 *Stability of the cyclic motion* - The initial velocity vector defines a reference closed
 1378 orbit in the median plane of the cyclotron dipole; a small perturbation in α or v
 1379 results in a new orbit *in the vicinity* of the reference. An axial velocity component v_y
 1380 on the other hand, causes the ion to drift away from the reference, vertically, linearly
 1381 with time, as there is no axial restoring force. The next Section will investigate the
 1382 necessary field property to ensure both horizontal and vertical confinement of the
 1383 cyclic motion in the vicinity of a reference orbit in the median plane.

1384 3.2.2 Weak Focusing

1385 In the early accelerated turns in a classical cyclotron (central region of the electro-
 1386 magnet, energy up to tens of keV/u), the accelerating electric field provides vertical
 1387 focusing for particles with proper RF phase [?, Sect. 8], whereas a flat magnetic field
 1388 with uniformity $dB/B < 10^{-4}$ is sufficient to maintain isochronism. Beyond this low
 1389 energy region however, at greater radii, a magnetic field gradient must be introduced
 1390 to ensure transverse stability: field must decrease with R .

Fig. 3.8 Moving frame
 ($M_0; s, x, y$) along the ref-
 erence circular orbit. The cur-
 vature $1/R_0$ is constant along
 the orbit and ($M_0; s, x, y$)
 can be considered equiva-
 lent to the cylindrical frame
 ($C; \theta, R_0, y$)



1391 Ion coordinates in the following are defined in the moving frame ($M_0; s, x, y$)
 1392 (Fig. 3.8), which moves along the reference orbit (radius R_0), with its origin M_0
 1393 the projection of ion location M on the reference orbit; the s axis is tangent to the
 1394 latter, the x axis is normal to s , the y axis is normal to the bend plane. Median-plane
 1395 symmetry of the field is assumed, thus the radial field component $B_R|_{y=0} = 0$ at all
 1396 R (Fig. 3.9).

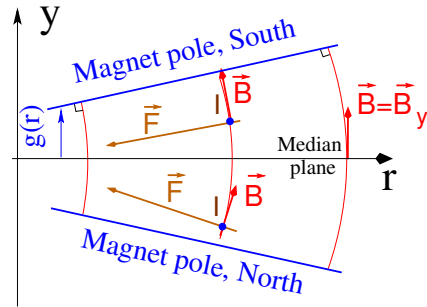
1397 Consider small motion excursions $x(t) = r(t) - R_0 \ll R_0$; introduce Taylor
 1398 expansion of the field components,

$$\begin{aligned}
 B_y(R_0 + x) &= B_y(R_0) + x \left. \frac{\partial B_y}{\partial R} \right|_{R_0} + \frac{x^2}{2!} \left. \frac{\partial^2 B_y}{\partial R^2} \right|_{R_0} + \dots \approx B_y(R_0) + x \left. \frac{\partial B_y}{\partial R} \right|_{R_0} \\
 B_R(0 + y) &= y \left. \frac{\partial B_R}{\partial y} \right|_0 + \frac{y^3}{3!} \left. \frac{\partial^3 B_R}{\partial y^3} \right|_0 + \dots \approx y \left. \frac{\partial B_y}{\partial R} \right|_{R_0} \\
 &= \underbrace{\left. \frac{\partial B_y}{\partial R} \right|_{R_0}}_{(3.7)}
 \end{aligned}$$

1399 Using these, and noting $(\dot{*}) = d(*)/dt$, the linear approximation of the differential
 1400 equations of motion in the moving frame writes

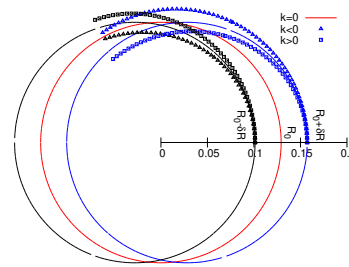
$$\begin{aligned}
 F_x = m\ddot{x} &= -qvB_y(R) + \frac{mv^2}{R_0 + x} \approx -qv \left(B_y(R_0) + \left. \frac{\partial B_y}{\partial R} \right|_{R_0} x \right) + \frac{mv^2}{R_0} \left(1 - \frac{x}{R_0} \right) \\
 \rightarrow m\ddot{x} &= -\frac{mv^2}{R_0^2} \left(\frac{R_0}{B_0} \left. \frac{\partial B_y}{\partial R} \right|_{R_0} + 1 \right) x \tag{3.8} \\
 F_y = m\ddot{y} &= qvB_R(y) = qv \left. \frac{\partial B_R}{\partial y} \right|_{y=0} y + \text{higher order} \rightarrow m\ddot{y} = qv \frac{\partial B_y}{\partial R} y
 \end{aligned}$$

Fig. 3.9 Axial motion stability requires proper shaping of field lines: B_y has to decrease with radius. The Laplace force pulls a positive charge with velocity pointing out of the page, at I, toward the median plane. Increasing the field gradient (k closer to -1, gap opening up faster) increases the focusing



1401

Fig. 3.10 Geometrical focusing: take $k=0$; two circular trajectories which start from $r = R_0 \pm \delta R$ (solid lines, going counter-clockwise) undergo exactly one oscillation around the reference orbit $r = R_0$. A negative k (triangles), for axial focusing, decreases the radial convergence; a positive k (square markers) increases the radial convergence - and increases vertical divergence

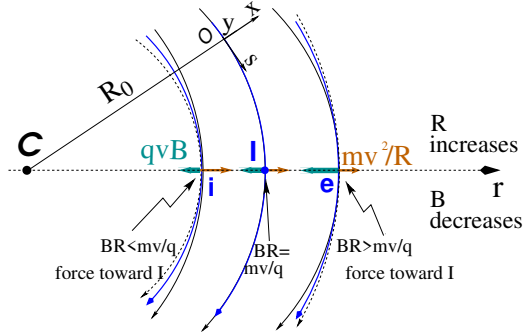


1402 Note $B_y(R_0) = B_0$ and introduce

$$\omega_R^2 = \omega_{\text{rev}}^2 \left(1 + \frac{R_0}{B_0} \frac{\partial B_y}{\partial R} \right), \quad \omega_y^2 = -\omega_{\text{rev}}^2 \frac{R_0}{B_0} \frac{\partial B_y}{\partial R} \tag{3.9}$$

1403 substitute in Eqs. 3.8, this yields

Fig. 3.11 Radial motion stability. Trajectory arcs at $p = mv$ are represented: case of $k = 0$ (thin black lines), of $-1 < k < 0$ (thick blue lines), and of $k = -1$ (dashed concentric circles). k decreasing towards -1 reduces the geometrical focusing, increases axial focusing. The resultant of the Laplace and centrifugal forces, $F_t = -qvB + mv^2/r$, is zero at I, motion is stable if F_t is toward I at i , i.e. $qvB_i < mv^2/R_i$, and toward I as well at e , i.e. $qvB_e > mv^2/R_e$



$$\ddot{x} + \omega_R^2 x = 0 \quad \text{and} \quad \ddot{y} + \omega_y^2 y = 0 \quad (3.10)$$

1404 A restoring force (linear terms in x and y , Eq. 3.10) arises from the radially varying
1405 field, characterized by a field index

$$k = \frac{R_0}{B_0} \left. \frac{\partial B_y}{\partial R} \right|_{R=R_0, y=0} \quad (3.11)$$

1406 *Radial stability*: radially this force adds to the geometrical focusing (curvature term
1407 “1” in ω_R^2 , Eq. 3.9, Fig. 3.10). In the weakly decreasing field $B(R)$ an ion with mo-
1408 mentum $p = mv$ moving in the vicinity of the R_0 -radius reference orbit experiences
1409 in the moving frame a resultant force $F_t = -qvB + m \frac{v^2}{r}$ (Fig. 3.11) of which the
1410 (outward) component $f_c = m \frac{v^2}{r}$ decreases with r at a higher rate than the decrease
1411 of the Laplace (inward) component $f_B = -qvB(r)$. In other words, radial stability
1412 requires BR to increase with R , $\frac{\partial BR}{\partial R} = B + R \frac{\partial B}{\partial R} > 0$, this holds in particular at R_0 ,
1413 thus $1 + k > 0$.

1414 *Axial stability* requires a restoring force directed toward the median plane. Refer-
1415 ring to Fig. 3.9, this means $F_y = -a \times y$ (with a a positive quantity) and thus $B_R < 0$,
1416 at all $(r, y \neq 0)$. This is achieved by designing a guiding field which decreases with
1417 radius, $\frac{\partial B_R}{\partial y} < 0$. Referring to Eq. 3.11 this means $k < 0$.

1418 From these radial and axial constraints the condition of “weak focusing” for
1419 transverse motion stability around the circular equilibrium orbit results, namely,

$$-1 < k < 0 \quad (3.12)$$

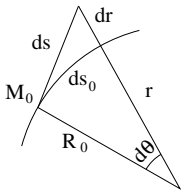
1420 Note regarding the geometrical focusing: the focal distance associated with the
1421 curvature of a magnet of arc length \mathcal{L} is obtained by integrating $\frac{d^2 x}{ds^2} + \frac{1}{R_0^2} x = 0$ and
1422 identifying with the focusing property $\Delta x' = -x/f$, namely,

$$\Delta x' = \int \frac{d^2 x}{ds^2} ds \approx \frac{-x}{R^2} \int ds = \frac{-x \mathcal{L}}{R^2}, \text{ thus } f = \frac{R^2}{\mathcal{L}} \quad (3.13)$$

1423 *Isochronism*: the axial focusing constraint, B decreasing with R , contributes break-
 1424 ing the isochronism (in addition to the effect of the mass increase) by virtue of
 1425 $\omega_{\text{rev}} \propto B$.

1426 Paraxial Transverse Coordinates

1427 Introduce the path variable s as the independent variable in Eq. 3.10 and neglect the
 1428 transverse velocity components ($1 + \frac{x}{R_0} \approx 1$, $y \ll 0$) so that

$$ds = [r^2(s)d\theta^2 + dr^2 + dy^2]^{1/2} \approx |\mathbf{v}|dt \quad (3.14)$$


1429 thus the equations of motion in the moving frame (Eq. 3.10) take the form

$$\frac{d^2 x}{ds^2} + \frac{1+k}{R_0^2} x = 0 \quad \text{and} \quad \frac{d^2 y}{ds^2} - \frac{k}{R_0^2} y = 0 \quad (3.15)$$

1430 Given $-1 < k < 0$ the motion is that of a harmonic oscillator, in both planes, with
 1431 respective restoring constants $(1+k)/R_0^2$ and $-k/R_0^2$, both positive quantities. The
 1432 solution is a sinusoidal motion,

$$\begin{cases} r(s) - R_0 = x(s) = x_0 \cos \frac{\sqrt{1+k}}{R_0}(s - s_0) + x'_0 \frac{R_0}{\sqrt{1+k}} \sin \frac{\sqrt{1+k}}{R_0}(s - s_0) \\ r'(s) = x'(s) = -x_0 \frac{\sqrt{1+k}}{R_0} \sin \frac{\sqrt{1+k}}{R_0}(s - s_0) + x'_0 \cos \frac{\sqrt{1+k}}{R_0}(s - s_0) \end{cases} \quad (3.16)$$

$$\begin{cases} y(s) = y_0 \cos \frac{\sqrt{-k}}{R_0}(s - s_0) + y'_0 \frac{R_0}{\sqrt{-k}} \sin \frac{\sqrt{-k}}{R_0}(s - s_0) \\ y'(s) = -y_0 \frac{\sqrt{-k}}{R_0} \sin \frac{\sqrt{-k}}{R_0}(s - s_0) + y'_0 \cos \frac{\sqrt{-k}}{R_0}(s - s_0) \end{cases} \quad (3.17)$$

1434 Radial and axial wave numbers can be introduced,

$$\nu_R = \frac{\omega_R}{\omega_{\text{rev}}} = \sqrt{1+k} \quad \text{and} \quad \nu_y = \frac{\omega_y}{\omega_{\text{rev}}} = \sqrt{-k} \quad (3.18)$$

1435 *i.e.*, the number of sinusoidal oscillations of the paraxial motion about the reference
 1436 circular orbit over a turn, respectively radial and axial. Both are less than 1: there
 1437 is less than one sinusoidal oscillation in a revolution. In addition, as a result of the
 1438 revolution symmetry of the field,

$$\nu_R^2 + \nu_y^2 = 1 \quad (3.19)$$

1439 *Off-Momentum Orbit*

In a structure with revolution symmetry, the equilibrium trajectory at momentum $\begin{cases} p_0 \\ p = p_0 + \Delta p \end{cases}$ is at radius $\begin{cases} R_0 \text{ with } B_0 R_0 = \frac{p_0}{q} \\ R \text{ with } BR = \frac{p}{q} \end{cases}$, where $\begin{cases} B = B_0 + \left(\frac{\partial B}{\partial x}\right)_0 \Delta x + \dots \\ R = R_0 + \Delta x \end{cases}$
 On the other hand

$$BR = \frac{p}{q} \Rightarrow \left[B_0 + \left(\frac{\partial B}{\partial x}\right)_0 \Delta x + \dots \right] (R_0 + \Delta x) = \frac{p_0 + \Delta p}{q}$$

1440 which, neglecting terms in $(\Delta x)^2$, and given $B_0 R_0 = \frac{p_0}{q}$, leaves $\Delta x \left[\left(\frac{\partial B}{\partial x}\right)_0 R_0 + B_0 \right] = \frac{\Delta p}{q}$. With $k = \frac{R_0}{B_0} \left(\frac{\partial B}{\partial x}\right)_0$ this yields

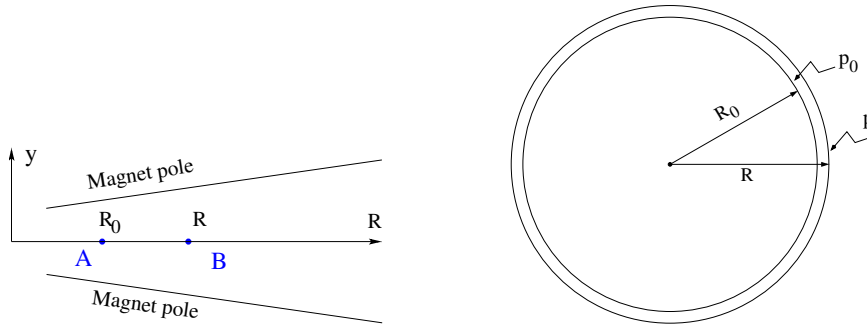


Fig. 3.12 The equilibrium radius at location A is R_0 , momentum is p_0 , rigidity is $B_0 R_0$. The equilibrium radius at B is R , momentum p , rigidity BR

1441

$$\Delta x = D \frac{\Delta p}{p_0} \quad \text{with} \quad D = \frac{R_0}{1+k} \quad \text{the dispersion function} \quad (3.20)$$

1442 The dispersion D is an s -independent quantity as a result of the revolution symmetry
 1443 of the field (k and $R=p/qB$ are s -independent).

1444 To the first order in the coordinates, the vertical coordinates $y(s)$, $y'(s)$ (Eq. 3.17)
 1445 are unchanged under the effect of a momentum offset, the horizontal trajectory angle
 1446 $x'(s)$ (Eq. 3.16) is unchanged as well (the circular orbits are concentric, Fig. 3.12)
 1447 whereas $x(s)$ satisfies

$$x(s, p_0 + \Delta p) = x(s, p_0) + \Delta p \left. \frac{\partial x}{\partial p} \right|_{s, p_0} = x(s, p_0) + D \frac{\Delta p}{p_0} \quad (3.21)$$

1448 *Orbit and revolution period lengthening*

1449 A δp momentum offset results in (Eq. 3.20)

$$\frac{\delta C}{C} = \frac{\delta R}{R} = \frac{\delta x}{R} = \alpha \frac{\delta p}{p} \quad \text{with} \quad \alpha = \frac{1}{1+k} = \frac{1}{\gamma^2 R} \quad (3.22)$$

1450 with α the momentum compaction, a positive quantity: orbit length increases with
 1451 momentum. Substituting $\frac{\delta \beta}{\beta} = \frac{1}{\gamma^2} \frac{\delta p}{p}$, the change in revolution period $T_{\text{rev}} = C/\beta c$
 1452 with momentum writes

$$\frac{\delta T_{\text{rev}}}{T_{\text{rev}}} = \frac{\delta C}{C} - \frac{\delta \beta}{\beta} = \left(\alpha - \frac{1}{\gamma^2} \right) \frac{\delta p}{p} \quad (3.23)$$

1453 Given that $-1 < k < 0$ and $\gamma \gtrsim 1$, it results that $\alpha - 1/\gamma^2 > 0$: the revolution period
 1454 increases with energy, the increase in radius is faster than the velocity increase.

1455 3.2.3 Quasi-Isochronous Resonant Acceleration

1456 The energy W of an accelerated ion (in the non-relativistic energy domain of the
 1457 classical cyclotron) satisfies the frequency dependence

$$W = \frac{1}{2} m v^2 = \frac{1}{2} m (2\pi R f_{\text{rev}})^2 = \frac{1}{2} m \left(2\pi R \frac{f_{\text{rf}}}{h} \right)^2 \quad (3.24)$$

1458 Observe in passing: given the cyclotron size (radius R), f_{rf} and h set the limit for
 1459 the acceleration range. The revolution frequency decreases with energy and the
 1460 condition of synchronism with the oscillating voltage, $f_{\text{rf}} = h f_{\text{rev}}$, is only fulfilled
 1461 at that particular radius where $\omega_{\text{rf}} = qB/m$ (Fig. 3.13-left). The out-phasing $\Delta\phi$ of
 1462 the RF at ion arrival at the gap builds-up turn after turn, decreasing in a first stage
 1463 (towards lower voltages in Fig. 3.13-right) and then increasing back to $\phi = \pi/2$ and
 1464 beyond towards π . Beyond $\phi = \pi$ the RF voltage is decelerating.

1465 With ω_{rev} constant between two gap passages, differentiating $\phi(t)$ (Eq. 3.2) yields
 1466 $\dot{\phi} = \omega_{\text{rf}} - \omega_{\text{rev}}$. Between two gap passages on the other hand, $\Delta\phi = \dot{\phi}\Delta T = \dot{\phi}T_{\text{rev}}/2 =$
 1467 $\dot{\phi} \frac{\pi R}{v}$, yielding a phase-shift of

$$\text{half-turn} \quad \Delta\phi = \pi \left(\frac{\omega_{\text{rf}}}{\omega_{\text{rev}}(R)} - 1 \right) = \pi \left(\frac{m\omega_{\text{rf}}}{qB(R)} - 1 \right) \quad (3.25)$$

1468 The out-phasing is thus a gap-after-gap, cumulative effect. Due to this the classical
 1469 cyclotron requires quick acceleration (small number of turns), which means high
 1470 voltage (tens to hundreds of kVolts). As expected, with ω_{rf} and B constant, ϕ presents
 1471 a minimum ($\dot{\phi} = 0$) at $\omega_{\text{rf}} = \omega_{\text{rev}} = qB/m$ where exact isochronism is reached
 1472 (Fig. 3.13). The upper limit to ϕ is set by the condition $\Delta W > 0$: acceleration.

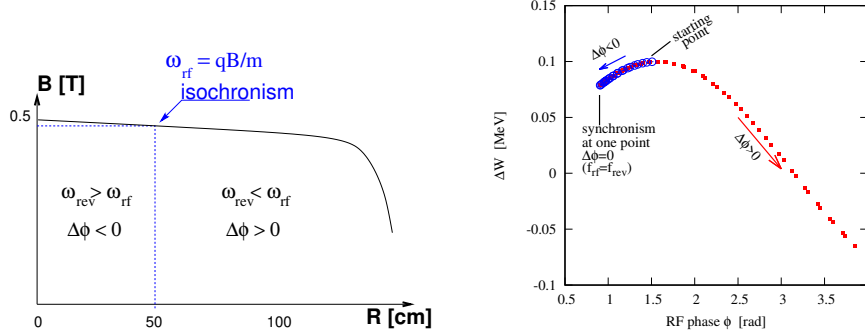
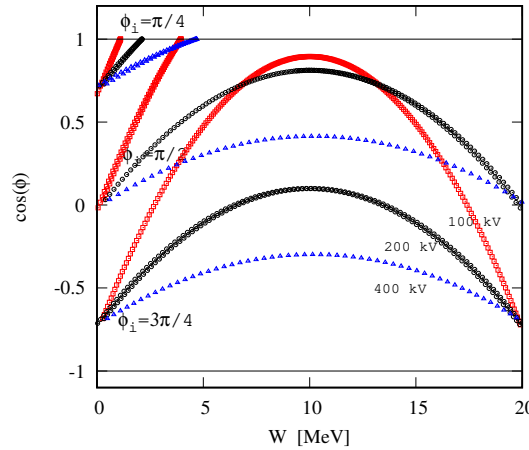


Fig. 3.13 Left: a sketch of the synchronism condition at one point ($h=1$ assumed). Right: the span in phase of the energy gain $\Delta W = q\hat{V} \sin \phi$ (Eq. 3.2) over the acceleration cycle

Fig. 3.14 A graph of the cyclotron equation (Eq. 3.26), for three different accelerating voltages: 100, 200 and 400 kV/gap (respectively square, circle and triangle markers). The sole settings resulting in $-1 < \cos \phi(E) < 1$, $\forall E$, allow complete acceleration to top energy. $\phi_i = \pi/4$ at injection for instance, does not (upper three curves). $\phi_i = 3\pi/4$ works (lower three curves), with as low as 100 kV/gap



1473 The cyclotron equation determines the achievable energy range, depending on
 1474 the injection energy E_i , the RF phase at injection ϕ_i , the RF frequency ω_{rf} and gap
 1475 voltage \hat{V} . It writes [?]

$$\cos \phi = \cos \phi_i + \pi \left[1 - \frac{\omega_{rf}}{\omega_{rev}} \frac{E + E_i}{2M} \right] \frac{E - E_i}{q\hat{V}} \quad (3.26)$$

1476 Equation 3.26 is represented in Fig. 3.14 for various values of the peak voltage
 1477 and phase at injection ϕ_i . M [eV/c²] and E [eV] are respectively the rest mass and
 1478 relativistic energy, $q\hat{V}$ is expressed in electron-volts, the index i denotes injection
 1479 parameters.

1480 3.2.4 Beam Extraction

1481 From $R = p/qB$ and assuming $B(R) \approx \text{constant}$ (this is legitimate as k is normally
1482 small), in the non-relativistic approximation ($W \ll M$, $W = p^2/2M$) one gets

$$\frac{dR}{R} = \frac{1}{2} \frac{dW}{W} \quad (3.27)$$

1483 Integrating yields

$$R^2 = R_i^2 \frac{W}{W_i} \quad (3.28)$$

1484 with R_i, W_i initial conditions. From Eqs. 3.27, 3.28, assuming $W_i \ll W$ and constant
1485 acceleration rate dW such that $W = n dW$ after n turns, one gets the scaling laws

$$R \propto \sqrt{n}, \quad dR \propto \frac{R}{W} \propto \frac{1}{R} \propto dW, \quad \frac{dR}{dn} = \frac{R}{2n} \quad (3.29)$$

1486 The turn separation dR is proportional to the energy gain per turn and inversely
1487 proportional to the orbit radius.

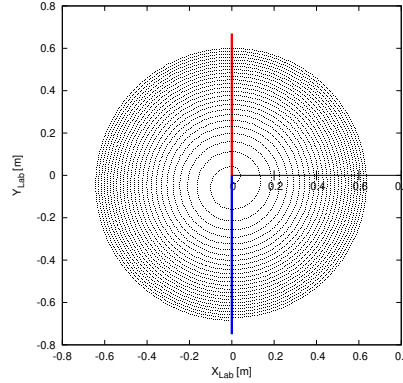


Fig. 3.15 The radial distance between successive turns decreases with energy, in inverse proportion to the orbit radius. The red and blue segments here figure the accelerating gap

1488 The radial distance between successive turns decreases with energy, toward zero
1489 (Fig. 3.15), eventually resulting in insufficient spacing for insertion of an extraction
1490 septum.

1491 *Orbit modulation*

1492 Consider an ion bunch injected in the cyclotron with some (x_0, x'_0) conditions in
1493 the vicinity of the reference orbit, and assume slow acceleration. While accelerated
1494 the bunch undergoes an oscillatory motion around the equilibrium orbit (Eq. 3.16).
1495 Observed at the extraction septum this oscillation modulates the distance of the

1496 bunch to the local equilibrium orbit, moving it outwards or inwards depending on
 1497 the turn number, which modulates the distance between the accelerated turns. This
 1498 effect can be resorted to, so to increase the separation between the final two turns
 1499 and so enhance the extraction efficiency [?].

1500 3.2.5 Spin Dance

1501 *“Much of the physics of spin motion can be illustrated using the simplest model of a*
 1502 *storage ring consisting of uniform horizontal bending and no straight sections.”* [?].

1503 By virtue of this statement, a preliminary introduction to spin motion in magnetic
 1504 fields is given in the present chapter. In support to this in addition, comes the fact that
 1505 cyclotrons happened to be the first circular machines to accelerate polarized beams
 1506 (first acceleration of polarized beams had happened earlier in the 1960s, using
 1507 electrostatic columns at voltage generators, when polarized proton and deuteron
 1508 sources began operating [?]).

1509 The magnetic field \mathbf{B} of the cyclotron dipole exerts a torque on the spin angular
 1510 momentum \mathbf{S} of an ion, causing it to precess following the Thomas-BMT differential
 1511 equation [?]

$$\frac{d\mathbf{S}}{dt} = \mathbf{S} \times \underbrace{\frac{q}{m} [(1 + G)\mathbf{B}_{\parallel} + (1 + G\gamma)\mathbf{B}_{\perp}]}_{\omega_{\text{sp}}} \quad (3.30)$$

1512 where t is the time; ω_{sp} the precession vector: a combination of \mathbf{B}_{\parallel} and \mathbf{B}_{\perp} compo-
 1513 nents of \mathbf{B} respectively parallel and orthogonal to the ion velocity vector. G is the
 1514 gyromagnetic anomaly,

1515 $G=1.7928474$ (proton), -0.178 (Li), -0.143 (deuteron), -4.184 (^3He) ...

1516 \mathbf{S} in this equation is in the ion rest frame, all other quantities are in the laboratory
 1517 frame.

1518 In the case of an ion moving in the median plane of the dipole, $\mathbf{B}_{\parallel} = 0$, thus the
 1519 precession axis is parallel to the magnetic field vector, \mathbf{B}_y , so that $\omega_{\text{sp}} = \frac{q}{m} (1 +$
 1520 $G\gamma)\mathbf{B}_y$. The spin precession angle over a trajectory arc \mathcal{L} is

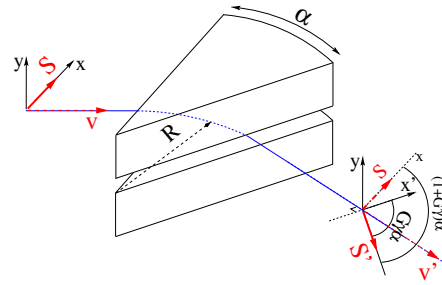
$$\theta_{\text{sp, Lab}} = \frac{1}{v} \int_{(\mathcal{L})} \omega_{\text{sp}} ds = (1 + G\gamma) \frac{\int_{(\mathcal{L})} B ds}{BR} = (1 + G\gamma)\alpha \quad (3.31)$$

1521 with α the velocity vector precession (Fig. 3.16). The precession angle in the moving
 1522 frame (the latter rotates by an angle α along \mathcal{L}) is

$$\theta_{\text{sp}} = G\gamma\alpha \quad (3.32)$$

1523 thus the number of 2π spin precessions per ion orbit around the cyclotron is $G\gamma$. By
 1524 analogy with the wave numbers (Eq. 3.18) this defines the “spin tune”

Fig. 3.16 Spin and velocity vector precession in a constant field, from \mathbf{S} to \mathbf{S}' and \mathbf{v} to \mathbf{v}' respectively. In the moving frame the spin precession along the arc $\mathcal{L} = R\alpha$ is $G\gamma\alpha$, in the laboratory frame the spin precesses by $(1 + G\gamma)\alpha$



$$\nu_{\text{sp}} = G\gamma \quad (3.33)$$

1525 3.3 Exercises

1526 Note: some of the input data files for these simulations are available in zgoubi
 1527 sourceforge repository at
 1528 https://sourceforge.net/p/zgoubi/code/HEAD/tree/branches/exemples/book/zgoubiMaterial/cyclotron_classical/

1529 3.1 Modeling a Cyclotron Dipole: Using a Field Map

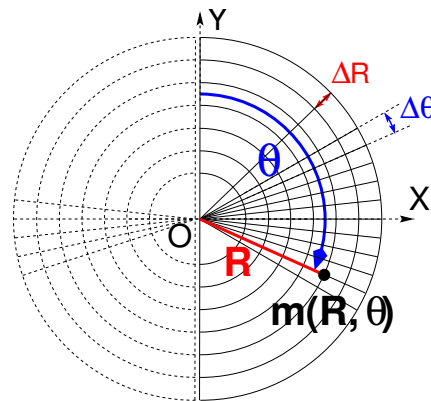
1530 Solution: page 300

1531 In this exercise, ion trajectories are ray-traced, various optical properties addressed
 1532 in the foregoing are recovered, using a field map to simulate the cyclotron dipole.
 1533 Fabricating that field map is a preliminary step of the exercise.

1534 The interest of using a field map is that it is an easy way to account for fancy
 1535 magnet geometries and fields, including field gradients and possible defects. A
 1536 field map can be generated using mathematical field models, or from magnet com-
 1537 putation codes, or from magnetic measurements. The first method is used, here.
 1538 TOSCA[MOD.MOD1=22.1] keyword [?, cf. INDEX] is used to ray-trace through
 1539 the map.

1540 *Working hypotheses:* A 2-dimensional $m(R, \theta)$ polar meshing of the median plane
 1541 is considered (Fig. 3.17). It is defined in a $(O; X, Y)$ frame and covers an angular
 1542 sector of a few tens of degrees. The mid-plane field map is the set of values $B_Z(R, \theta)$
 1543 at the nodes of the mesh. During ray-tracing, TOSCA[MOD.MOD1=22.1] extrapolates
 1544 the field along 3D space (R, θ, Z) ion trajectories from the 2D polar map [?].

Fig. 3.17 Principle of a 2D field map in polar coordinates, covering a 180° sector (over the right hand side dee). The mesh nodes $m(R, \theta)$ are distant ΔR radially, $\Delta\theta$ azimuthally. The map is used twice to cover the 360° cyclotron dipole as sketched here, while allowing insertion of an accelerating gap between the two dees



1545 (a) Construct a 180° two-dimensional map of a median plane field $B_Z(R, \theta)$,
 1546 proper to simulate the field in a cyclotron as sketched in Fig. 3.1. Use one of
 1547 the following two methods: either (i) write an independent program, or (ii) use
 1548 zgoubi and its analytical field model DIPOLE, together with the keyword OP-
 1549 TIONS[CONSTY=ON] [?, cf. INDEX].

1550 Besides: use a uniform mesh (Fig. 3.17) covering from $R_{\min}=1$ to $R_{\max}=76$ cm,
 1551 with radial increment $\Delta R = 0.5$ cm, azimuthal increment $\Delta\theta = 0.5$ [cm]/ R_0 with R_0

1552 some reference radius (say, 50 cm, in view of subsequent exercises), and constant
 1553 axial field $B_Z = 5$ kG. The appropriate 6-column formatting of the field map data
 1554 for TOSCA[MOD.MOD1=22.1] to read is the following:

1555 $R \cos \theta, Z, R \sin \theta, BY, BZ, BX$

1556 with θ varying first, R varying second; Z is the vertical direction (normal to the map
 1557 mesh), $Z \equiv 0$ in the present case. Note that proper functioning of TOSCA requires
 1558 the field map to begin with the following line of numerical values:

1559 Rmin [cm] ΔR [cm] $\Delta \theta$ [deg] Z [cm]

1560 Produce a graph of the $B_Z(R, \theta)$ field map content.

1561 (b) Ray-trace a few concentric circular mid-plane trajectories centered on the
 1562 center of the dipole, ranging in $10 \leq R \leq 80$ cm. Produce a graph of these concentric
 1563 trajectories in the $(O; X, Y)$ laboratory frame.

1564 Initial coordinates can be defined using OBJET, particle coordinates along tra-
 1565 jectories during the stepwise ray-tracing can be logged in zgoubi.plt by setting IL=2
 1566 under TOSCA. In order to find the Larmor radius corresponding to a particular
 1567 momentum, the matching procedure FIT can be used. In order to repeat the latter for
 1568 a series of different momenta, REBELOTE[IOPT=1] can be used.

1569 Explain why it is possible to push the ray-tracing beyond the 76 cm radial extent
 1570 of the field map.

1571 (c) Compute the orbit radius R and the revolution period T_{rev} as a function of
 1572 kinetic energy W or rigidity BR . Produce a graph, including for comparison the
 1573 theoretical dependence of T_{rev} .

1574 (d) Check the effect of the density of the mesh (the choice of ΔR and $\Delta \theta$ values,
 1575 *i.e.*, the number of nodes $N_\theta \times N_R = (1 + \frac{180^\circ}{\Delta \theta}) \times (1 + \frac{80 \text{ cm}}{\Delta R})$), on the accuracy of the
 1576 trajectory and time-of-flight computation.

1577 (e) Check the effect of the integration step size on the accuracy of the trajectory
 1578 and time-of-flight computation, by considering a small $\Delta s = 1$ cm and a large
 1579 $\Delta s = 10$ cm, at 200 keV and 5 MeV (proton), and comparing with theory.

1580 (f) Consider a periodic orbit, thus its radius R should remain unchanged after
 1581 stepwise integration of the motion over a turn. However, the size Δs of the numerical
 1582 integration step has an effect on the final value of the radius:

1583 For two different cases, 200 keV (a small orbit) and 5 MeV (a larger one), provide a
 1584 graph of the dependence of the relative error $\delta R/R$ after one turn, on the integration
 1585 step size Δs (consider a series of Δs values in a range $\Delta s : 0.1 \text{ mm} \rightarrow 20 \text{ cm}$).
 1586 REBELOTE[IOPT=1] do-loop can be used to repeat the one-turn raytracing with
 1587 different Δs .

1588 3.2 Modeling a Cyclotron Dipole: Using an Analytical Field Model

1589 Solution: page 308

1590 This exercise is similar to exercise 3.1, yet using the analytical modeling DIPOLE,
 1591 instead of a field map. DIPOLE provides the Z -parallel median plane field $\mathbf{B}(R, \theta, Z =$
 1592 $0) \equiv \mathbf{B}_Z(R, \theta, Z = 0)$ at the projected $m(R, \theta, Z = 0)$ ion location (Fig. 3.18), while
 1593 $\mathbf{B}(R, \theta, Z)$ at particle location is obtained by extrapolation.

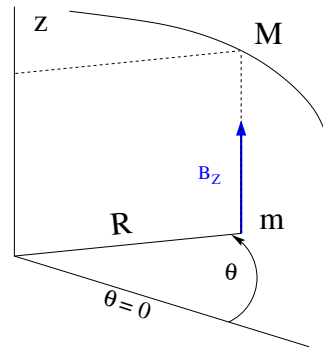


Fig. 3.18 DIPOLE provides the value $B_Z(m)$ of the median plane field at m , projection of particle position $M(R, \theta, Z)$ in the median plane. $\mathbf{B}(R, \theta, Z)$ is obtained by extrapolation

1594 (a) Simulate a 180° sector dipole; DIPOLE requires a reference radius [?,
1595 Eqs. 6.3.19-21], noted R_0 here; for the sake of consistency with other exercises,
1596 it is suggested to take $R_0 = 50$ cm. Take a constant axial field $B_Z = 5$ kG.

1597 Explain the various data that define the field simulation in DIPOLE: geometry,
1598 role of R_0 , field and field indices, fringe fields, integration step size, etc.

1599 Produce a graph of $B_Z(R, \theta)$.

1600 (b) Repeat question (b) of exercise 3.1.

1601 (c) Repeat question (c) of exercise 3.1.

1602 (d) As in question (e) of exercise 3.1, check the effect of the integration step size
1603 on the accuracy of the trajectory and time-of-flight computation.

1604 Repeat question (f) of exercise 3.1.

1605 (e) From the two series of results (exercise 3.1 and the present one), comment on
1606 various pros and cons of the two methods, field map versus analytical field model.

1607 3.3 Resonant Acceleration

1608 Solution: page 312

1609 Based on the earlier exercises, using indifferently a field map (TOSCA) or an
1610 analytical model of the field (DIPOLE), introduce a sinusoidal voltage between the
1611 two dees, with peak value 100 kV. Assume that ion motion does not depend on RF
1612 phase: the boost through the gap is the same at all passes, use CAVITE[IOPT=3] [?,
1613 cf. INDEX] for that. Note that using CAVITE requires prior PARTICUL in order to
1614 specify ion species and data, necessary to compute the energy boost (Eq. 3.2).

1615 (a) Accelerate a proton with initial kinetic energy 20 keV, up to 5 MeV, take
1616 harmonic $h=1$. Produce a graph of the accelerated trajectory in the laboratory frame.

1617 (b) Provide a graph of the proton momentum p and total energy E as a function
1618 of its kinetic energy, both from this numerical experiment (ray-tracing data can be
1619 stored using FAISTORE) and from theory, all on the same graph.

1620 (c) Provide a graph of the normalized velocity $\beta = v/c$ as a function of kinetic
1621 energy, both numerical and theoretical, and in the latter case both classical and
1622 relativistic.

1623 (d) Provide a graph of the relative change in velocity $\Delta\beta/\beta$ and orbit length $\Delta C/C$
 1624 as a function of kinetic energy, both numerical and theoretical. From their evolution,
 1625 conclude that the time of flight increases with energy.

1626 (e) Repeat the previous questions, assuming a harmonic $h=3$ RF frequency.

1627 3.4 Spin Dance

1628 Solution: page 316

1629 Cyclotron modeling in the present exercise can use Exercise 3.1 or Exercise 3.2
 1630 technique (*i.e.*, a field map or an analytical field model), indifferently.

1631 (a) Add spin transport, using SPNTRK [?, *cf.* INDEX]. Produce a listing
 1632 (zgoubi.res) of a simulation, including spin outcomes.

1633 Note: PARTICUL is necessary here, for the spin equation of motion (Eq. 3.30) to
 1634 be solved [?, Sect. 2]. SPNPRT can be used to have local spin coordinates listed in
 1635 zgoubi.res (at the manner that FAISCEAU lists local particle coordinates).

1636 (b) Consider proton case, take initial spin longitudinal, compute the spin precession
 1637 over one revolution, as a function of energy over a range 12 keV \rightarrow 5 MeV. Give
 1638 a graphical comparison with theory.

1639 FAISTORE can be used to store local particle data, which include spin coordi-
 1640 nates, in a zgoubi.fai style output file. IL=2 [?, *cf.* INDEX] (under DIPOLE or
 1641 TOSCA, whichever modeling is used) can be used to obtain a print out of particle
 1642 and spin motion data to zgoubi.plt during stepwise integration.

1643 (c) Inject a proton with longitudinal initial spin S_i . Give a graphic of the lon-
 1644 gitudinal spin component value as a function of azimuthal angle, over a few turns
 1645 around the ring. Deduce the spin tune from this computation. Repeat for a couple of
 1646 different energies.

1647 Place both FAISCEAU and SPNPRT commands right after the first dipole sector,
 1648 and use them to check the spin rotation and its relationship to particle rotation, right
 1649 after the first passage through that first sector.

1650 (d) Spin dance: the input data file optical sequence here is assumed to model a
 1651 full turn. Inject an initial spin at an angle from the horizontal plane (this is in order
 1652 to have a non-zero vertical component), produce a 3-D animation of the spin dance
 1653 around the ring, over a few turns.

1654 (e) Repeat questions (b-d) for two additional ions: deuteron (much slower spin
 1655 precession), ${}^3\text{He}^{2+}$ (much faster spin precession).

1656 3.5 Synchronized Spin Torque

1657 Solution: page 322

1658 A synchronized spin kick is superimposed on orbital motion. An input data file for
 1659 a complete cyclotron is considered as in question 3.4 (d), for instance six 60 degree
 1660 DIPOLEs, or two 180 degree DIPOLEs.

1661 Insert a local spin rotation of a few degrees around the longitudinal axis, at the
 1662 end of the optical sequence (*i.e.*, after one orbit around the cyclotron). SPINR can be
 1663 used for that, rather than a local magnetic field, so to avoid any orbital effect. Track
 1664 4 particles on their respective equilibrium orbit, with energies 0.2, 108.412, 118.878
 1665 and 160.746 MeV.

1666 Produce a graph of the motion of the vertical spin component S_y along the circular
1667 orbit.

1668 Produce a graph of the spin vector motion on a sphere.

1669 3.6 Weak Focusing

1670 Solution: page 325

1671 (a) Consider a 60° sector as in earlier exercises (building a field map and using
1672 TOSCA as in exercise 3.1, or using DIPOLE as in exercise 3.2), construct the sector
1673 accounting for a non-zero radial index k in order to introduce axial focusing, say
1674 $k = -0.03$, assume a reference radius R_0 for a reference energy of 200 keV (R_0 and
1675 B_0 are required in order to define the index k , Eq. 3.11). Ray-trace that 200 keV
1676 reference orbit, plot it in the lab frame: make sure it comes out as expected, namely,
1677 constant radius, final and initial angles zero.

1678 (b) Using FIT[2], find and plot the radius dependence of orbit rigidity, $BR(R)$,
1679 from ray-tracing over a BR range covering 20 keV to 5 MeV; superpose the theoretical
1680 curve. REBELOTE[IOPT=1] can be used to perform the scan.

1681 (c) Produce a graph of the paraxial axial motion of a 1 MeV proton, over a few
1682 turns (use IL=2 under TOSCA, or DIPOLE, to have step by step particle and field
1683 data logged in zgoubi.plt). Check the effect of the focusing strength by comparing
1684 the trajectories for a few different index values, including close to -1 and close to 0.

1685 (d) Produce a graph of the magnetic field experienced by the ion along these
1686 trajectories.

1687 3.7 Loss of Isochronism

1688 Solution: page 334

1689 Compare on a common graphic the revolution period $T_{\text{rev}}(R)$ for a field index
1690 value $k \approx -0.95, -0.5, -0.03, 0^-$. The scan method of exercise 3.6, based on
1691 REBELOTE[IOPT=1] preceded by FIT[2], can be referred to.

1692 3.8 Ion Trajectories

1693 Solution: page 336

1694 In this exercise individual ion trajectories are computed. DIPOLE or TOSCA
1695 magnetic field modeling can be used, indifferently. No acceleration here, ions circle
1696 around the cyclotron at constant energy.

1697 (a) Produce a graph of the horizontal $x(s)$ and vertical $y(s)$ trajectory coordinates
1698 of an ion with rigidity close to $BR(R_0)$ (R_0 is the reference radius in the definition of
1699 the index k), over a few turns around the cyclotron. From the number of turns, give
1700 an estimate of the wave numbers. Check the agreement with the expected $\nu_R(k)$,
1701 $\nu_y(k)$ values (Eq. 3.18).

1702 (b) Consider now protons at 1 MeV and 5 MeV, far from the reference energy
1703 $E(R_0)$; the wave numbers change with energy: consistency with theory can be
1704 checked. Find their theoretical values, compare with numerical outcomes.

1705 (c) Consider proton, 200 keV energy, plot as a function of s the difference between
1706 $x(s)$ from raytracing and its values from Eq. 3.16. Same for $y(s)$ compared to Eq. 3.17.

1707 IL=2 can be used to store in zgoubi.plt the step-by-step particle coordinates across
1708 DIPOLE.

1709 (d) Perform a scan of the wave numbers over 200 keV–5 MeV energy inter-
1710 val, computed using OBJET[KOBJ=5] and MATRIX[IORD=1,IFOC=11], or OB-
1711 JET[KOBJ=6] and MATRIX[IORD=2,IFOC=11], together with REBELOTE[IOPT=1]
1712 to repeat MATRIX for a series of energy values.

1713 3.9 RF Phase at the Accelerating Gap

1714 Solution: page 342

1715 Consider the cyclotron model of exercise 3.6: field index $k = -0.03$ defined at
1716 $R_0 = 50$ cm, field $B_0 = 5$ kG on that radius. two dees, double accelerating gap.

1717 Accelerate a proton from 1 to 5 MeV: get the turn-by-turn phase-shift at the gaps;
1718 use CAVITE[IOPT=7] to simulate the acceleration. Compare the half-turn $\Delta\phi$ so
1719 obtained with the theoretical expectation (Eq. 3.25). Produce similar graphs $B(R)$
1720 and $\Delta W(\phi)$ to Fig. 3.13.

1721 Accelerate over more turns, observe the particle decelerating.

1722 3.10 The Cyclotron Equation

1723 Solution: page 344

1724 The cyclotron model of exercise 3.3 is considered: two dees, double accelerating
1725 gap, uniform field $B = 5$ kG, no field gradient needed here (no vertical motion).

1726 (a) Set up an input data file for the simulation of a proton acceleration from
1727 0.2 to 20 MeV. In particular, assume that $\cos(\phi)$ reaches its maximum value at
1728 $W_m = 10$ MeV; find the RF voltage frequency from $d(\cos \phi)/dW = 0$ at W_m .

1729 (b) Give a graph of the energy-phase relationship (Eq. 3.26), for $\phi_i = \frac{3\pi}{4}, \frac{\pi}{2}, \frac{\pi}{4}$,
1730 from both simulation and theory.

1731 3.11 Cyclotron Extraction

1732 Solution: page 346

1733 (a) Acceleration of a proton in a uniform field $B = 5$ kG is first considered (field
1734 hypotheses as in exercise 3.3). RF phase is ignored: CAVITE[IOPT=3] can be used
1735 for acceleration. Take a 100 kV gap voltage.

1736 Compute the distance ΔR between turns, as a function of turn number and of
1737 energy, over the range $E : 0.02 \rightarrow 5$ MeV. Compare graphically with theoretical
1738 expectation.

1739 (b) Assume a beam with Gaussian momentum distribution and *rms* momentum
1740 spread $\delta p/p = 10^{-3}$. An extraction septum is placed half-way between two successive
1741 turns, provide a graph of the percentage of beam loss at extraction, as a function of
1742 extraction turn number. COLLIMA can be used for that simulation and for particle
1743 counts, it also allows for possible septum thickness.

1744 (c) Repeat (a) and (b) considering a field with index: take for instance $B_0 = 5$ kG
1745 and $k = -0.03$ at $R_0 = R(0.2 \text{ MeV}) = 12.924888$ cm.

1746 (d) Investigate the effect of injection conditions (Y_i, T_i) on the modulation of the
1747 distance between turns.

1748 Try and confirm numerically that, with slow acceleration, the oscillation is mini-
 1749 mized for an initial $|T_i| = \left| \frac{x_0 v_R}{R} \right|$ (after Ref. [?, p. 133]).

1750 3.12 Acceleration and Extraction of a 6-D Polarized Bunch

1751 Solution: page 351

1752 The cyclotron simulation hypotheses of exercise 3.10-a are considered; account
 1753 or $k = -0.02$ field index.

1754 Add a short “high energy” extraction line, say 1 meter, following REBELOTE in
 1755 the optical sequence, ending up with a “Beam_Dump” MARKER for instance.

1756 (a) Create a 1,000 ion bunch with the following initial parameters:

1757 - random Gaussian transverse phase space densities, centered on the equilibrium
 1758 orbit, truncated at 3 sigma, normalized *rms* emittances $\varepsilon_Y = \varepsilon_Z = 1 \pi \mu\text{m}$, both
 1759 emittances matched to the 0.2 MeV orbit optics,

1760 - uniform bunch momentum density $0.2 \times (1 - 10^{-3}) \leq p \leq 0.2 \times (1 + 10^{-3}) \text{ MeV}$,
 1761 matched to the dispersion, namely (Eq. 3.21), $\Delta x = D \frac{\Delta p}{p}$,

1762 - random uniform longitudinal distribution $-0.5 \leq s \leq 0.5 \text{ mm}$,

1763 Note: two ways to create this object are, (i) using MCOBJET[KOBJ=3] which
 1764 generates a random distribution, or (ii) using OBJET[KOBJ=3] to read an external
 1765 particle coordinate file.

1766 Add spin tracking request (SPNTRK), all initial spins normal to the bend plane.

1767 Produce a graph of the three initial 2-D phase spaces: (Y,T), (Z,P), $(\delta l, \delta p/p)$,
 1768 matched to the 200 keV periodic optics. Provide Y, Z, dp/p, δl and S_Z histograms
 1769 (HISTO can be used), check the distribution parameters.

1770 (b) Accelerate this polarized bunch to 20 MeV, using the following RF conditions:

1771 - 200 kV peak voltage,

1772 - RF harmonic 1,

1773 - initial RF phase $\phi_i = \pi/4$.

1774 Produce a graph of the three phase spaces as observed downstream of the extrac-
 1775 tion line. Provide the Y, Z, dp/p, δl and S_Z histograms. Compare the distribution
 1776 parameters with the initial values.

1777 What causes the spins to spread away from vertical?